Vienna Congress on Recent Advances in
Earthquake Engineering and Structural Dynamics 2013 (VEESD 2013)
C. Adam, R. Heuer, W. Lenhardt & C. Schranz (eds)
28-30 August 2013, Vienna, Austria
Paper No. 193

Influence of coupling on the displacement capacities of URM piers – comparison of experimental results with existing recommendations

S. Petry[1], K. Beyer[1]

[1] Earthquake Engineering and Structural Dynamics Laboratory (EESD), School of Architecture, Civil and Environmental Engineering (ENAC), École Polytechnique Fédérale de Lausanne (EPFL), Switzerland

Abstract. In existing European recommendations the drift capacity of unreinforced masonry (URM) piers is estimated as a function of the failure mode, aspect ratio and/or axial load ratio. The empirical relationships are based on a set of results from quasi-static cyclic tests on single URM piers, which were tested simulating either double-fixed or cantilever boundary conditions. In modern URM structures, the URM piers are often connected by reinforced concrete (RC) slabs which provide enough stiffness and strength to impose a certain rotational restraint to the piers. In this paper we determine typical boundary conditions and apply them within a series of quasi-static cyclic tests of URM piers. Some preliminary results are presented and compared to existing recommendations for modern European masonry. Differences between the experimental results and the recommendations are reported and tendencies discussed.

Keywords: Seismic testing; Coupling influence; Displacement capacity; Unreinforced masonry;

1 INTRODUCTION

Modern Swiss construction combines often unreinforced masonry (URM) elements with reinforced concrete (RC) elements. For example, residential buildings are often constructed using vertical URM piers connected by RC slabs. When such buildings are subjected to lateral loading, the RC slabs, which possesses a significant out-of-plane stiffness, partially restrains the rotation of the piers and a certain coupling between vertical piers and horizontal slab takes place. Depending on the stiffness and strength of the slab, the amount of coupling can vary significantly and influences thus more or less the rotational restraint at top of the piers.

In order to obtain a better understanding of these modern mixed URM-RC structures, an ongoing research project at the EPFL is dedicated to the structural behaviour and interaction of the different elements, for instance the coupling introduced through RC slabs. This article discusses the influence of the coupling on the deformation capacities of URM piers. It is shown that depending on the location of the pier, i.e. whether the pier is an internal or external pier, the effect of the coupling changes. Within the project, a series of quasi-static cyclic tests on identical URM piers was conducted with different boundary conditions such as to simulate internal and external piers. Results of this testing series are presented and compared to existing recommendations. The article concludes with a discussion on the drift capacities given by codes.

2 DETERMINATION OF THE BOUNDARY CONDITIONS

2.1 Influence of the coupling on the moment and axial load profiles of internal piers

Modern masonry structures in Switzerland feature typically RC slabs, which provide sufficient in-plane rigidity to enforce equal horizontal displacement onto all piers of one story. The out-of-plane

stiffness and strength of the slab are limited but not negligible. Priestley et al. (2007), for instance, suggest including the slabs as one-dimensional RC beam elements in equivalent frame models of URM structures with an effective beam width $b_{cb,eff}$ of twice to three times the wall thickness t_w. However, these recommendations for the effective slab width are based on engineering judgment and to the author's knowledge they have never been validated against experimental results. In Figure 1, the axial load and moment profile in piers are plotted for two symmetrical structures assuming first an effective beam width of $b_{cb,eff} = t_w$ and then $b_{cb,eff} = 3t_w$. It can be noticed that the coupling assumption affects particularly the moment profile of the internal pier at ground floor, while the axial load of the internal pier remains unaffected. The internal pier is connected to one coupling element at each side. If we assume a symmetric coupling from both sides, the double coupling moment is introduced into the pier, while the shear forces coming from each coupling element cancel each other out and do not cause a change in axial force in the pier.

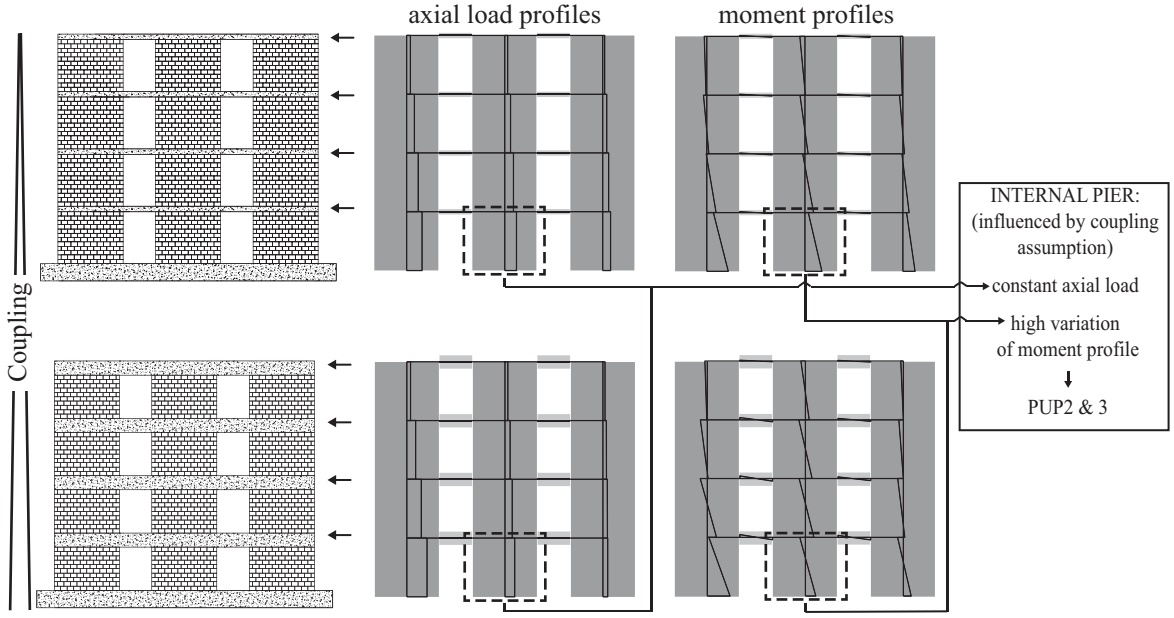

Figure 1. Influence of the coupling assumption on the axial load and moment profile of an internal pier at ground floor level.

The external pier, on the contrary, is only connected to one coupling element, hence the introduced coupling moment is less and the shear force coming from the coupling beam changes the axial load in the external pier (Figure 1). It can be noticed that the external pier is susceptible to the loading direction. Figure 2 shows the moment profile and axial load profile for an effective beam width of $b_{cb,eff} = 3t_w$. The change of axial load in the external pier is related to so-called overturning moment as shown in Figure 2. Accordingly, the left external pier is subjected to an increased axial load and the zero moment height is higher on the compression side of the structure. In contrast, the external pier on the so-called tension side of the structure is subjected to a lower axial load and its zero moment height is reduced.

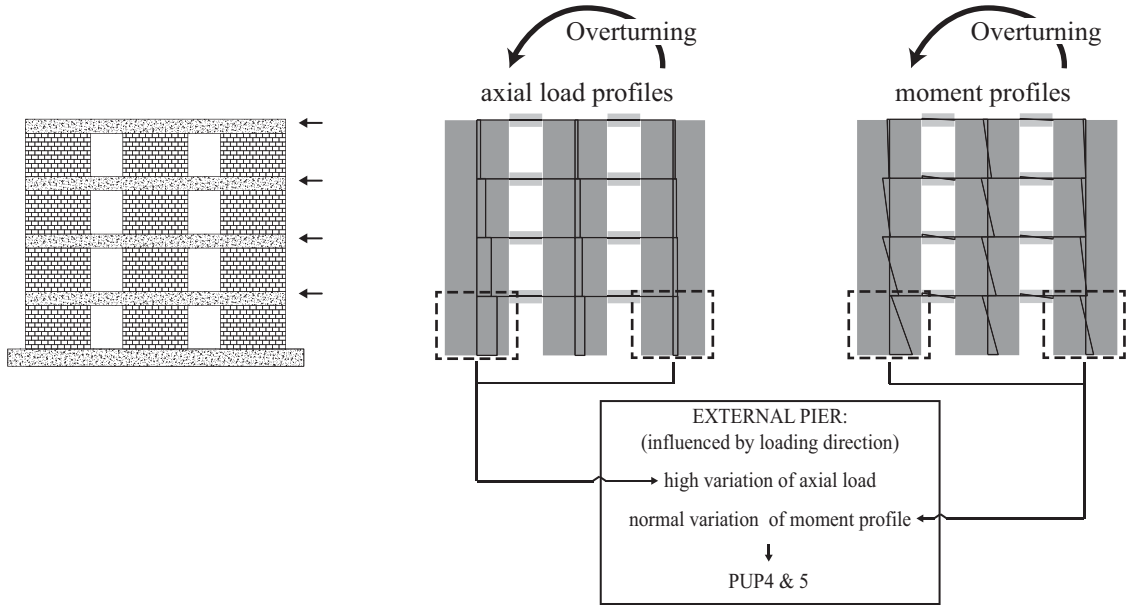

Figure 2. Influence of the loading direction on the axial load and moment profile of an external pier at ground floor level.

2.2 Chosen boundary conditions for PUP2 to PUP5

According to the conclusions on the coupling influence, we decided to simulate the different degrees of coupling in controlling the zero moment height ratio H_0/H where H is the height of one pier, i.e. the storey height. Therefore, the forces of the two vertical actuators $F_{ver,1}$ and $F_{ver,2}$, as shown in Figure 3, were coupled linearly to the force of the horizontal actuator F_{hor}:

$$F_{ver,1,2} = \frac{N}{2} \pm C_1 \cdot F_{hor} \tag{1}$$

with N representing the total axial load and C_1 representing a constant which depends on the chosen zero moment height ratio H_0/H. In this way we were able to assure a constant normal force and a constant ratio between the top and bottom moment during testing.

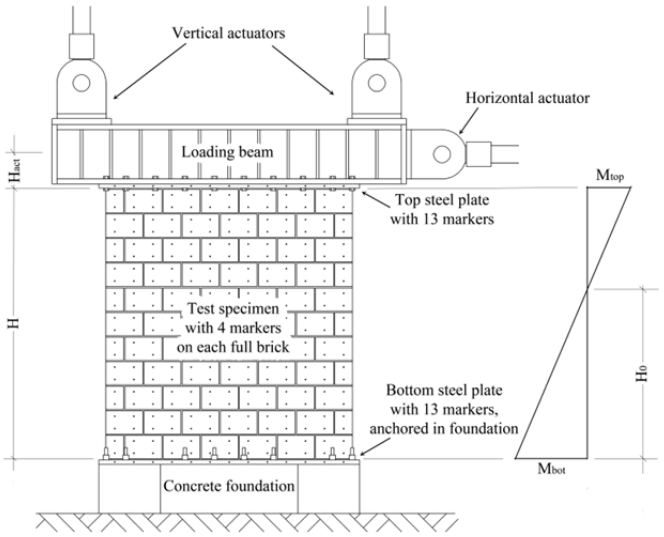

Figure 3. Test setup with layout of LEDs for optical measurements.

In the previous section, we showed that the piers were differently affected by the coupling in dependence of their position within the building, e.g. Figures 1 and 2. The first test PUP1 was a reference test which applied standard double-fixed boundary conditions to the pier. This test and the last (PUP6), which combined different boundary conditions in the two directions of loading, will not be subject of this paper. In order to simulate an internal pier, two piers – PUP2 and PUP3 – were tested with an identical axial load ratio of $\sigma_0/f_u = 0.18$ at two different zero moment height ratios of $H_0/H = 0.75$ and 1.5. The two zero moment height ratios represent different degrees of coupling and correspond for the reference building approximately to assumed effective slab widths of $3t_w$ and t_w, respectively. The axial stress σ_0 corresponds to the axial load N divided by the cross section of the piers A and f_u represents the compression strength of the investigated masonry. With the next two piers we aimed at simulating an external pier. Accordingly one pier – PUP4 – was tested with an increased axial load ratio of $\sigma_0/f_u = 0.26$ and an increased zero moment height ratio of $H_0/H = 1.5$, while the other pier – PUP5 – was tested with $\sigma_0/f_u = 0.09$ and $H_0/H = 0.75$. The boundary conditions are summarized in Table 1.

Table 1. Boundary conditions for PUP2-5.

Specimen	Degree of axial load	Normal stress ratio σ_0 / f_u	Degree of coupling	Zero moment height H_0
PUP2	Intermediate	0.18	High to intermediate	$0.75H$
PUP3	Intermediate	0.18	Intermediate	$1.5H$
PUP4	High	0.26	Intermediate	$1.5H$
PUP5	Low	0.09	High to intermediate	$0.75H$

3 QUASI-STATIC CYCLIC TESTS ON MASONRY PIERS

3.1 Investigated masonry and pier dimensions

The investigated URM piers represent typical modern Swiss masonry and were constructed with a typical modern Swiss hollow-core clay brick. The compression strength of the brick parallel to perforation was 35 MPa. As mortar, a commercial cement mortar mixture was taken, WEBER MUR MAXIT 920, which is widely used all over Switzerland. The head and bed joint thicknesses were 10 to 12 mm and were fully mortared. Compression tests on mortar prisms, which were taken during construction and tested at a similar age than the corresponding piers, resulted in a mean compression strength of 11 MPa. All piers were identical and the dimensions of the piers were 2.01 m x 2.25 m x 0.20 m (length x height x thickness). From material tests on the masonry, the mean compressive strength was determined at $f_u = 5.87$ MPa and the friction and cohesion of the mortar-brick interfaces as $\mu = 0.91$ and $c = 0.28$ MPa, respectively.

3.2 Testing procedure and loading history

All tests were performed applying the following procedure: (0) Zero measurements were taken before any of the three actuators was connected to the test unit (load step LS0). (1) The vertical actuators were fixed to the loading beam at the top of the pier. (2) The vertical force was applied by means of the two vertical actuators (LS1). The forces applied by the two actuators were equal ($F_{ver,1} = F_{ver,2} = N/2$); the resulting vertical force acted therefore at the centre line of the pier. (3) After applying the vertical load, the horizontal actuator was fixed to the loading beam. (4) Once the horizontal actuator was connected to the loading beam, the control functions for the vertical actuators were changed to the

control functions as indicated in Equation (1). (5) The lateral loading history was started (LS2 – end). A load step of the drift-controlled loading history corresponds to the peak of one half-cycle. At each load step, the loading was stopped, cracks were marked and photos were taken. The amplitudes of the half-cycles corresponded to the following drift levels: 0.025%, 0.05%, 0.1%, 0.15%, 0.2%, 0.3%, 0.4%, 0.6%, 0.8%, 1.0%. Cycles with amplitudes limited by forces, which are often included at the beginning of a loading history, were omitted in order to simplify the comparison of different test units within this test series.

3.3 Resulting force and drift capacity

For all the test units, the loading was continued until the piers were no longer able to carry the applied vertical load *N*, i.e., when axial load failure was attained. Nevertheless, herein this article the ultimate drift δ_u is determined at horizontal load failure, i.e., when the vertical force capacity dropped to 80% of the peak strength. This definition corresponds to the definition of the limit state "Near Collapse" as defined in Eurocode 8, Part 3 (CEN, 2004; Frumento, et al., 2009). In Figure 4.b to Figure 7.b the characteristic points are marked with an A for the peak load, B for the horizontal load failure (80% of peak strength) and C for the axial load failure. All piers were subjected to fully reversed cycles and the ultimate drift δ_u is taken as the minimum drift of both directions. When the axial load failure was attained before horizontal load failure, the maximum drift of the same direction is taken as ultimate drift value. The observed failure mechanisms, lateral drifts and peak loads are summarized in Table 2. A photo of each pier after axial load failure is shown in Figure 4.a to Figure 7.a and the corresponding boundary conditions are shown in Figure 4.c to Figure 7.c.

Table 2. Test results for PUP2-5.

Specimen	Failure mechanism	Peak load A+/-		Horizontal failure B+/-	Maximum drift	**Ultimate drift**
		F_{peak}	δ_A	δ_B	δ_{max}	$\boldsymbol{\delta_u}$
PUP2	Diagonal shear	178 kN -164 kN	0.35 % -0.37 %	0.40 % -	0.41 % -0.38 %	**0.38 %**
PUP3	Flexural rocking	121 kN -115 kN	0.48 % -0.75 %	0.69 % -1.04 %	0.81 % -1.05 %	**0.69 %**
PUP4	Hybrid failure	145 kN -142 kN	0.27 % -0.36 %	0.35 % -	0.44 % -0.37 %	**0.35 %**
PUP5	Diagonal shear	135 kN -121 kN	0.37 % -0.53 %	0.56 % -0.54 %	0.58 % -0.54 %	**0.54 %**

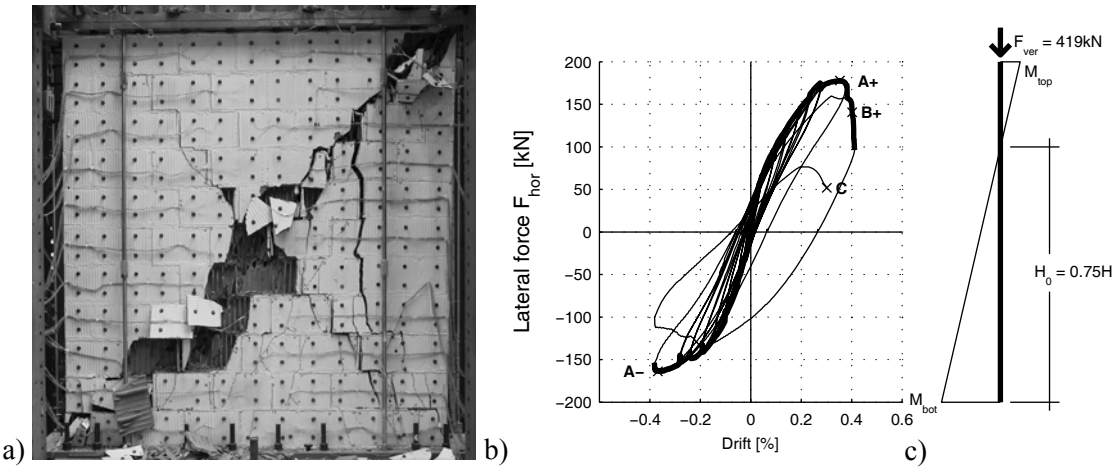

Figure 4. PUP2 (a) Photo after axial load failure, (b) displacement-force hysteresis and (c) moment diagram.

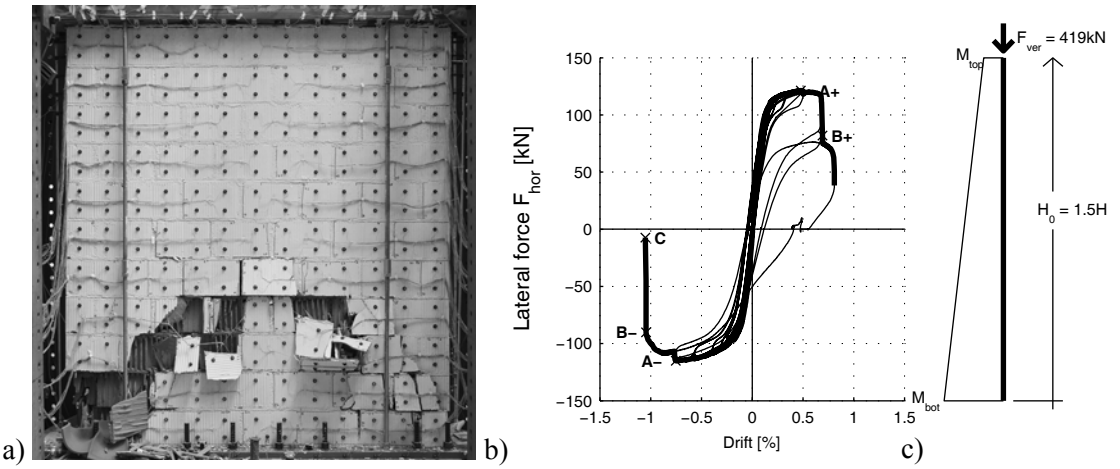

Figure 5. PUP3 (a) Photo after axial load failure, (b) displacement-force hysteresis and (c) moment diagram.

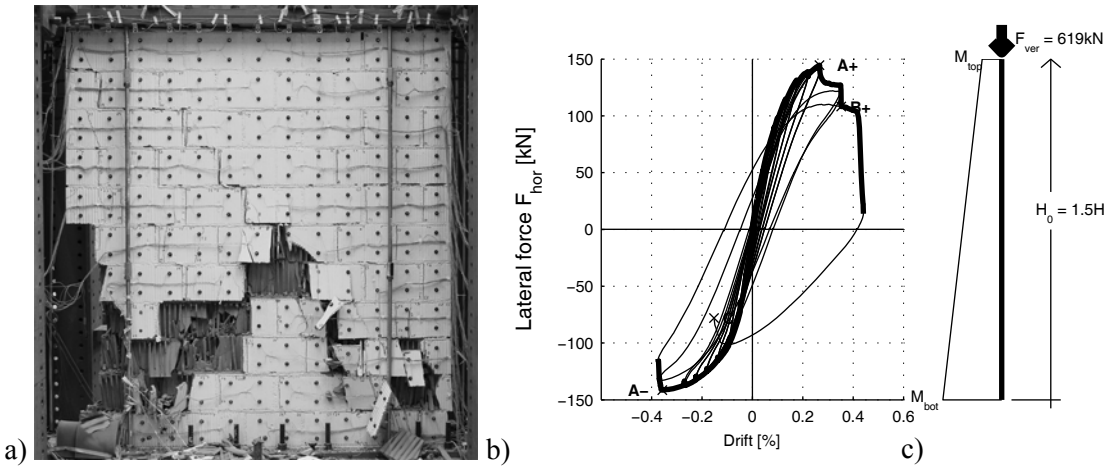

Figure 6. PUP4 (a) Photo after axial load failure, (b) displacement-force hysteresis and (c) moment diagram.

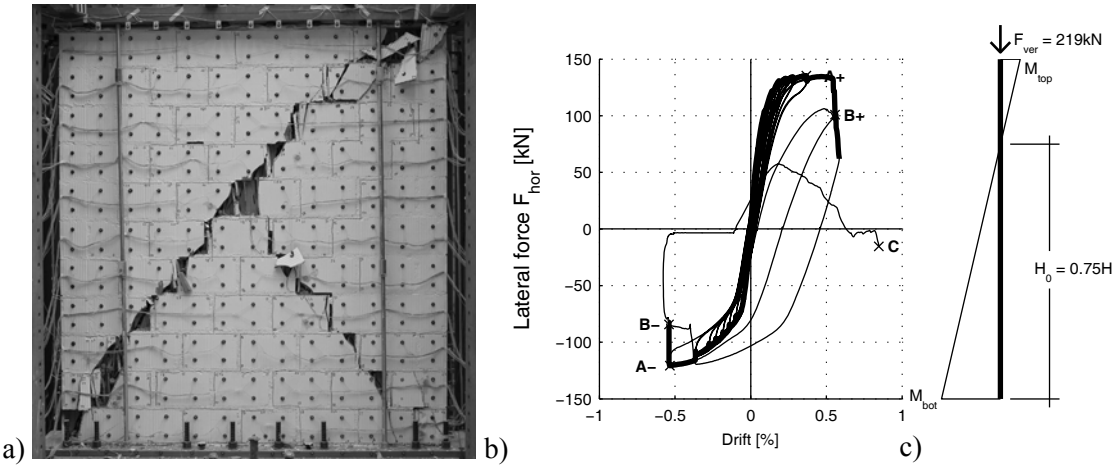

Figure 7. PUP5 (a) Photo after axial load failure, (b) displacement-force hysteresis and (c) moment diagram.

4 COMPARISON OF THE TEST RESULTS WITH EUROPEAN RECOMMENDATIONS

4.1 Prediction of the displacement capacity according to Eurocode 8 Part 3

In Eurocode 8, Part 3, the drift capacity of masonry piers is given as a function of the failure mode (CEN, 2004). Hence, first the flexural and shear capacity of the pier need to be determined according to Equations (2) and (3) and the smaller value of the two determines the failure mode.

$$V_f = \frac{LN}{2H_0}(1 - 1.15\,\vartheta_d) \tag{2}$$

$$V_{sh} = f_{vd} L' t \tag{3}$$

where L is the length of the pier and L' the length of the compression zone. The parameter ϑ_d accounts for the axial load ratio and is defined as:

$$\vartheta_d = \frac{N}{Ltf_d} \tag{4}$$

with f_d being the compression design strength of the masonry. The shear design strength f_{vd} can be computed as:

$$f_{vd} = f_{vd0} + 0.4\frac{N}{L't} \leq 0.065 f_{mk} \tag{5}$$

Once the failure mode is determined, the drift capacity corresponding to the limit state "Near Collapse" can be estimated as 4/3 x 0.4% = 0.53% for shear failure and 4/3 x 0.8% H_0/L = 1.07% H_0/L for flexural failure (CEN, 2004).

For a simple comparison of the test results with the recommendations of EC8, Part 3 (CEN, 2004), we assume a partial safety factor of unity for the material strength (γ_m = 1.0) and the characteristic compression strength is set equal to the mean compression strength $f_d = f_u$ = 5.87 MPa. The same is done for the cohesion, hence, $f_{vd0} = c$ = 0.28 MPa. To remove any unwarranted conservatism, we neglect the upper limit of 0.065 f_{mk} in Equation (5). The length of the compression zone L' can be computed considering a rectangular stress block with $f_c = 0.85 f_u$, e.g. (Priestley, et al., 2007):

$$N = 0.85 f_u \cdot L' t \tag{6}$$

Hence, Equation (5) can be simplified as follows:

$$V_{sh} = f_{vdo} \cdot \mathrm{L't} + 0.4N = N \cdot \frac{f_{vdo}}{0.85 f_u} + 0.4N \tag{7}$$

In Figure 8, the shear capacity, which is independent of the height of zero moment, is plotted for the investigated piers as a function of the axial load ratio σ_0/f_u. The flexural strength depends on the height of zero moment and therefore for each of the two different zero moment heights that were applied to the piers, the flexural strength is computed as a function of the axial load ratio. The minimum capacity controls the failure mode. It can be noticed that the failure mode is predicted correctly by the equations in Eurocode 8, Part 3 (abbreviated in the following as EC8 P3).

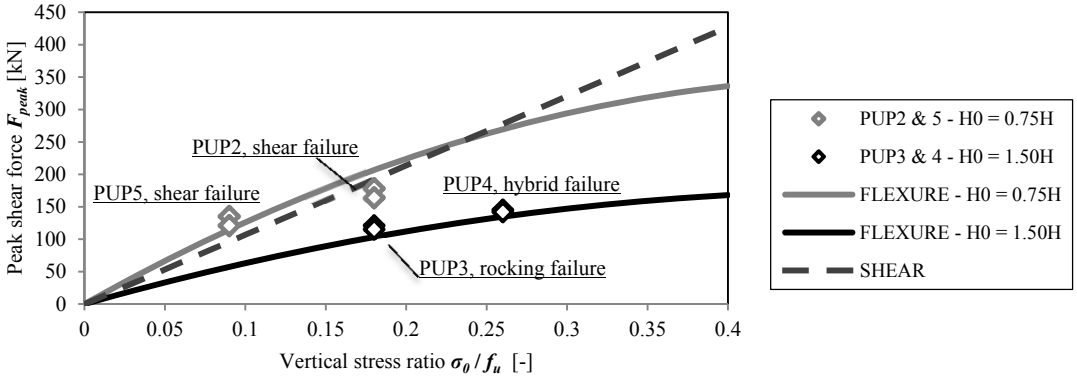

Figure 8. Predicted shear force and failure mode according to Eurocode 8, Part 3 (CEN, 2004) versus the tests results for PUP2 to PUP5.

4.2 Prediction of the displacement capacity according to SIA D 0237

In addition to the drift limits given by EC8 P3, in Switzerland the drift capacity of URM piers can be determined according to the SIA documentation SIA D 0237 (SIA, 2011) directly with the axial stress ratio σ_n/f_{xd}:

$$\delta_u = \delta_0 \cdot \left(1 - \frac{\sigma_n}{f_d}\right) \tag{8}$$

δ_u is the interstorey drift at ultimate stage, δ_0 can be taken as $\delta_0 = 0.8$, σ_n is the design value of the normal stress and f_{xd} is the design value of the compression strength of the masonry. In analogy to previous section, herein this article, the design values are replaced by the mean value obtained from the experimental tests. Thus, Equation (8) can be written as follows:

$$\delta_u = 0.8 \cdot \left(1 - \frac{\sigma_0}{f_u}\right) \tag{9}$$

Equation (8) is based on a series of tests of URM masonry piers, which were mainly tested under cantilever conditions and which corresponds accordingly to a zero moment height ratio of $H_0/H = 1.0$. For piers tested with double fixed conditions the SIA D 0237 emphasizes that lower drifts can be reached and recommends dividing the drift capacity δ_u by a factor of two:

$$\delta_u = 0.4 \cdot \left(1 - \frac{\sigma_0}{f_u}\right) \tag{10}$$

None of the herein presented piers PUP2 to PUP5 represents an exact double fixed or cantilever pier and no recommendation is given on how to deal with piers of intermediate conditions. Therefore, a conservative comparison is chosen herein and a linear interpolation between Equation (9) and (10) is considered for a zero moment height ratio $H_0/H < 1.0$:

$$\delta_u = 0.8 \cdot \frac{H_0}{H} \cdot \left(1 - \frac{\sigma_0}{f_u}\right) \tag{11}$$

4.3 Comparison

In Figures 9 and 10, the drift capacity according to EC8 P3 and SIA D 0237 is plotted as a function of the axial load ratio σ_0/f_u and the zero moment height ratio H_0/H. When comparing the predicted values with the test results from PUP2 to PUP5, it can be noticed that the drift capacity is mostly

overestimated. In the EC8 P3 (CEN, 2004), the drift capacity is determined as function of the failure mode and changes therefore only when the predicted failure mode changes. Nevertheless, even though PUP2 and PUP5 showed both a typical shear failure, both piers reached significant different drifts. There it is concluded that the assumption of identical drift capacity for identical failure mechanism is incorrect. However, also for PUP3 and PUP4, the drift capacity is significantly overestimated.

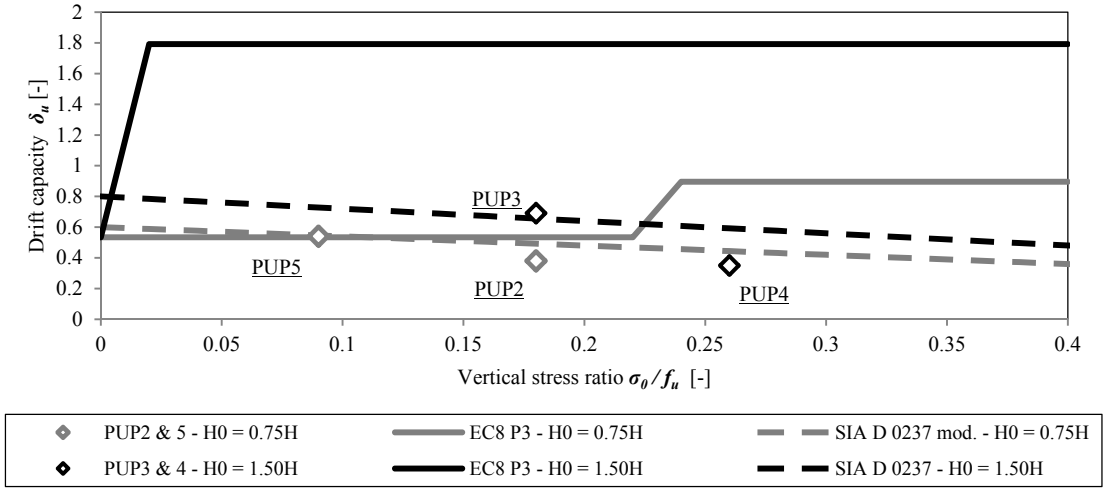

Figure 9. Predicted drift capacity as function of the axial stress ratio σ_0/f_u for the Eurocode 8 Part 3 (CEN, 2004) and the SIA D 0237 (SIA, 2011) versus the test results PUP2 to PUP5.

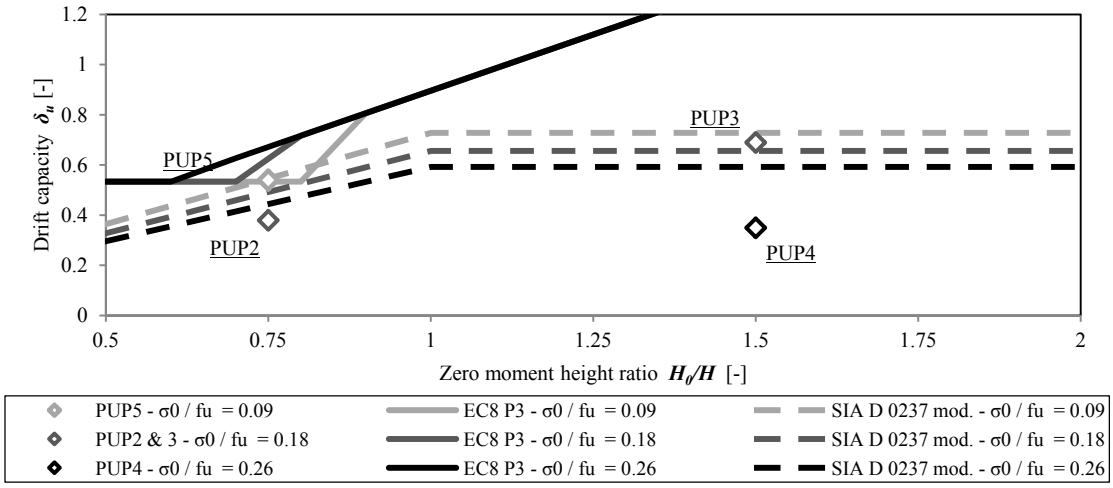

Figure 10. Predicted drift capacity as function of the zero moment height ratio H_0/H for the Eurocode 8 Part 3 (CEN, 2004) and the SIA D 0237 (SIA, 2011) versus the test results PUP2 to PUP5.

In SIA D 0237 (SIA, 2011), the drift capacity is given as a linear function of the axial stress ratio σ_0/f_u and, where no clear recommendation was given (for piers with $H_0/H < 1.0$), we assumed a linear interpolation for different height of zero moment ratios (see Equation (11)). In Figure 10, the drift capacity is plotted as a function of H_0/H for the three normal stress ratio of $\sigma_0/f_u = 0.09$, 0.18 and 0.26 and it can be noted that we get a better estimate of the drift capacity for $H_0/H < 1.0$. However, in Figure 9, it can be noticed that for both zero moment height ratios H_0/H, the SIA D 0237 underestimates the drift capacity for higher axial stress ratios σ_0/f_u. Equation (8) was determined empirically from a set of experiments (SIA, 2011).

5 CONCLUSIONS AND OUTLOOK

This article presents parts of the results of an ongoing research program on the structural behaviour of modern mixed structures composed with URM and RC elements. Herein this article the influence of the coupling on the displacement capacity of the URM piers is discussed. It is shown that depending on the position of the pier, e.g. internal or external pier, the assumption of the coupling and the loading direction changes the loading to which a pier is subjected. We identified exemplary boundary conditions for an internal and external pier and subjected a series of identical URM piers to quasi-static cyclic loading using these. From the tests, we determined the ultimate drift capacity according to the Eurocode 8 and further compared our results to the recommendations valid here in Switzerland.

While our test results showed a strong dependency on axial load ratio and zero moment height ratio, both factors are insufficiently considered in the EC8 P3 and the SIA D 0237. In the EC8 P3, the drift capacity is determined with respect to the failure mechanism and, only for flexural failure, the influence of the restraint is included. However, piers subjected to the same zero moment height ratio but different axial load ratios, showed similar failure mechanism but different drift capacities. Therefore, it is concluded that the pure dependency on failure modes is insufficient and would require so small drift capacities that it would be mostly too conservative. A comparison with the drift capacity given by the SIA D 0237 shows that better approximations can be achieved when the axial load ratio is included. Nevertheless, the curve overestimates the drift capacity for piers at higher axial load ratios. In addition, no clear recommendation is given on how to deal with the restrains. We obtained, for instance, a significant improvement in the drift estimate when including a linear dependency of the zero moment height ratio for $H_0/H < 1.0$.

In this article we presented part of a whole project which investigates the behaviour of modern URM structures in combination with RC elements. Additionally, models for predicting the strength-deformation relationships of spandrel elements, which were already tested experimentally (Beyer & Dazio, 2012), are developed in order to allow engineers to estimate the degree of coupling and therefore the height of zero moment in the piers.

6 ACKNOWLEDGEMENTS

The authors would like to thank Morandi Frères SA, Switzerland for the donation of the bricks. Great thanks are also due to the engineers and technicians of the laboratory. Without their technical and physical contribution, testing would simply not be feasible.

7 REFERENCES

Beyer, K. & Dazio, A., 2012. Quasi-static monotonic and cyclic tests on composite spandrels. *accepted in Earthquake Spectra,* 28(3), pp. 885-906.

CEN, 2004. *Eurocode 8: Design of structures for earthquake resistance - Part 3: Strengthening and repair of buildings EN 1998-3:2004.* Brussels: European Comittee for Standardization.

Frumento, S., Magenes, G., Morandi, P. & Calvi, G. M., 2009. *Interpretation of experimental shear tests on clay brick masonry walls and evaluation of q-factors for seismic design.* Pavia: IUSS Press.

Priestley, M. J. N., Calvi, G. M. & Kowalsky, M. J., 2007. *Displacement-Based Seismic Design of Structures.* Pavia: IUSS Press.

SIA, 2011. *SIA D 0237: Evaluation de la sécurité parasismique des bâtiments en maçonnerie.* Zürich: SGEB Société suisse du génie parasismique des bâtiments en maçonnerie.